J MATER SCI **41** (2006) 445–453

Synthesis, characterization and devitrification behaviour of an yttrium containing boroaluminate glass

N. HÉMONO, J. ROCHERULLÉ*, M. LE FLOCH, B. BUREAU
UMR CNRS 6512 Verres et Céramiques (LVC), Institut de Chimie de Rennes,
Université de Rennes I, Campus de Beaulieu, 35042 Rennes Cedex, France
E-mail: Jean.Rocherulle@univ-rennes1.fr

P. BÉNARD-ROCHERULLÉ
UMR CNRS 6511 Chimie du Solide et Inorganique Moléculaire (LCSIM), Institut de Chimie de Rennes, Université de Rennes I, Campus de Beaulieu, 35042 Rennes Cedex, France

The glass forming region in the B_2O_3-Al_2O_3-Y_2O_3 composition diagram has been determined by a melting and quenching procedure at temperatures up to 1800°C. Different physical characteristics (density, coefficient of thermal expansion, glass transition and crystallization peak temperatures) have been determined for a $35B_2O_3$-$40Al_2O_3$-$25Y_2O_3$ glass composition (in mol.%). By using a predictive model and some NMR structural data, different elastic moduli (Young's modulus, bulk modulus, shear modulus and Poisson's ratio) have been calculated. The devitrification behaviour has also been studied. Internal crystallization is the dominant mechanism and a new (Y,Al)BO_3 ternary phase has been characterized by X-ray powder diffraction. The temperature and time nucleation dependence have been determined from DTA experiments as well as the crystallization kinetics (i.e. the Avrami exponent and the activation energy for crystal growth). *© 2006 Springer Science + Business Media, Inc.*

1. Introduction

At the beginning of the 80's, the glass forming region, properties and structure have been studied for the La2O3-B_2O_3 binary diagram [1]. Stable liquid-liquid immiscibility exists for a wide composition range, thus homogeneous glasses can be obtained only for low (<2 mol.%) or high (>20 mol.%) La2O3 contents. However, for contents higher than 28 mol.%, $LaBO_3$ crystallizes during quenching. Moreover borate melts containing rare-earth ions smaller than Sm, namely Eu, Gd, Ho and Er cannot be vitrified [2]. Vibrational spectroscopies and solid-state nuclear magnetic resonance spectroscopy (NMR) indicate that these glasses primarily possess metaborate chains $(B_3O_6)_\infty$ that are tied together by highly coordinated La^{3+} ions. Described for their high-refractive index and low-dispersion optical applications, these glasses also have poor resistance to attack by aqueous solutions [1]. Nevertheless, it has been showed that the addition of Al_2O_3 improves the glass forming tendency and aqueous durability, increases the coefficient of thermal expansion and reduces the glass transition temperature (T_g) and the molar volume [3]. Furthermore, Brow and Tallant [4] have studied the polyhedral rearrangements in lanthanum aluminoborate glasses. They showed that tetrahedral aluminum sites substitute for the tetrahedral boron species to form modified $(AlB_2O_6)_\infty$ metaborate chains. However, cations with large electrostatic field strength, such as La^{3+}, stabilize the formation of more highly coordinated (five or six) aluminum. Consequently, yttrium should be considered as a reliable trivalent cation for glass synthesis. For that reason, Rutz *et al.* have studied the B_2O_3-Al_2O_3-Y_2O_3 ternary composition diagram. Homogeneous glasses can be obtained by melting at 1500°C in an electric furnace and quenching to room temperature compositions containing from 50 to 65 mol% B_2O_3 [5]. However, the maximum content in Al_2O_3 or Y_2O_3 oxides does not exceed 25 mol.% restraining the refractory character of these trivalent cations. As a consequence, the aim of this work was (i) to enlarge the glass forming region in the B_2O_3-Al_2O_3-Y_2O_3 composition diagram by a melting

---

*Author to whom all correspondence should be addressed.

0022-2461 © *2006 Springer Science + Business Media, Inc.*
DOI: 10.1007/s10853-005-2157-7

and quenching procedure at temperatures up to 1800°C (ii) to characterize a glass composition with the lowest available B_2O_3 content (iii) to study the devitrification behaviour of this glass matrix.

2. Experimental

2.1. Glass synthesis

Boric acid H_3BO_3 was previously melted at 700°C and quenched in order to obtain vitreous B_2O_3. Glasses were prepared from mixtures of this anhydrous B_2O_3 glass and reagent-grade of Al_2O_3 and Y_2O_3. The mixtures were heated at 1800°C in a molybdenum crucible by means of a high frequency device under a nitrogen atmosphere to prevent oxidation. Then the melts were quenched at room temperature in their own crucible. No significant loss of weight was observed during melting.

2.2. Glass characterization

Differential Thermal Analysis (DTA) experiments were performed with a TA Instruments Model SDT 2960. The glass sample was contained in a Pt pan, an empty Pt pan was used as the standard. Temperature calibration was carried out over a large range employing high purity materials improved by the ICTA. The overall accuracy of this instrument is expected to be within ±0.2 K. In the present work, heating rates in the range of 5 to 20°C/min were employed. The coefficient of thermal expansion (CTE) was measured by a TA Instruments Model TMA 2940, with a 5°C/min heating rate to 400°C and a preload force of 0.050 Newton. The density of the BAlY glass was measured by the Archimedes method using water as the suspending medium.

The ^{27}Al (I = 5/2) and ^{11}B (I = 3/2) single pulse NMR spectra were recorded at room temperature on a ASX 300 Bruker spectrometer operating at respectively 78.2 and 96.3 MHz with a 4 mm MAS probe spinning at 15 kHz. For this both quadrupolar nucleus a $\pi/12$ pulse length was chosen to fulfil the condition $\nu_{\mathrm{rf}} < \nu_{\mathrm{Q}}$ to avoid any line distortions and to ensure a possible quantification of the different sites [6]. The recycle delay was 1 s and the spectral width was 1 kHz to prevent the outer spinning side bands from folding back into the 15 kHz MAS spectrum. The external reference used for the ^{27}Al chemical shifts is $Al(NO_3)_3$ 1 M [6, 7], and $NaBH_4$ was used as secondary reference for 11B spectra [8].

The limits of the glass forming region were checked by X-ray powder diffraction. Data were collected with a PHILIPS diffractometer using Cu Kα radiation ($\lambda K\alpha_1$=1.5406 Å, $\lambda K\alpha_2$=1.5444Å) selected with a diffracted-beam graphite monochromator and the Bragg Brentano optics. The ICDD PDF database, available in the program search/match from the PC software package X'PERT supplied by PHILIPS, was interrogated in order to reveal possible isostructural chemically related compounds from the powder data sets of the crystalline phases obtained after the crystallization heat treatments.

3. Theoretical

3.1. Calculation of the elastic moduli

Makishima and Mackenzie [9] have elaborated a theory to predict the elastic moduli of oxide glasses. On this basis, when an ionic model is considered, the Young's modulus of a crystalline oxide is given by:

$$E = 2 \cdot \alpha U / r_0^3$$

where α is the Madelung constant, U the attraction electrostatic energy and r_0 is the interatomic distance. Because of the disordered structure of glass, it is difficult to adopt a meaningful Madelung constant as for a crystalline oxide. Instead of the Madelung energy per unit volume, Makishima *et al.* have considered the product of the dissociation energy per unit volume and a term without unit, relative to the packing density.

However, the agreement between calculation and experience was not always satisfying, it notably underestimated the highest experimental values. Rocherullé *et al.* [10] introduced some modifications in the expression of the packing factor in order to make better this theoretical calculation. Therefore, the Young's modulus can be stated as follows:

$$E = 2 \cdot C_{\mathrm{T}} \cdot G_{\mathrm{T}}$$

where C_{T} and G_{T} are the packing factor and the dissociation energy by unit volume for a polycomponent glass, respectively:

$$C_{\mathrm{T}} = \sum_i x_i C_i$$

$$G_{\mathrm{T}} = \sum_i x_i G_i$$

with x_i the molar fraction, C_i the packing factor and G_{i} the dissociation energy per unit volume associated to a compound A_aB_b. Those values must be calculated first by using the following formulas:

$$C_i = Z_i \frac{4\pi}{3} \frac{\left(a_{R_{\mathrm{A}}^3} + b_{R_{\mathrm{B}}^3}\right)}{V_i}$$

$$G_i = U_i \frac{\rho_i}{M_i}$$

where Z_i, V_i, U_i, ρi, M_i, R_A and R_B are the number of formulary units per unit cell, the molar volume, the dissociation energy per mole, the specific weight, the molecular weight and the Pauling's ionic radii of a crystalline compound A_aB_b, respectively.

Concerning the borate glasses, we must obviously take into account the fact that the coordination number of boron varies from 3 to 4 for the calculation of the elastic moduli. The G_i value for B_2O_3 is fairly high, but the Young's modulus of boric oxide glass is very low. This may be attributed to the structure of B_2O_3 glass with the weak binding forces between planes of interlinking BO_3 triangles compared to the three-dimensional linking (BO_4) bonds in the crystalline form. Thus, we must calculate two dissociation energies per unit volume, one for BO_3 (G_3) from the Young's modulus of the boric oxide glass and one for BO_4 (G_4) from thermodynamical data available for the crystalline form. From NMR experiments, we can know the different fraction of the boron coordination polyhedra and the dissociation energy per unit volume for a boron containing multicomponent glass can be expressed by:

$$G_{\mathrm{B_2O_3}} = \lambda G_4 + (1 - \lambda) G_3$$

γ being the BO_4 fraction in the glass.

Concerning the other moduli, the first Grüneisen rule gives the value of the bulk modulus, K, for a solid. The formulation is complex and requires knowledge of terms relative to the crystalline state. As for the calculation of E, terms relative to the vitreous state are difficult to evaluate; this is the reason for which it is interesting to replace them by the dissociation energy per unit volume and the packing factor. Makishima *et al.* [11] have shown that a linear relation exists between K and the $V_{\mathrm{T}}E$ product. Rocherullé *et al.* [10] have verified that such a relation exists for the function $K = f(C_{\mathrm{T}}E)$, thus the bulk modulus can be expressed by:

$$K = 2\alpha_{V_{\mathrm{T}}^2 G_{\mathrm{T}}}$$

with the proportionality constant $\alpha = 1.08$. Furthermore the shear modulus, S, and the Poisson's ratio, μ, which are linked to E and K, can be expressed according to G_{T}, V_{T} and α as follows:

$$S = \frac{6\alpha_{V_{\mathrm{T}}^2 G_{\mathrm{T}}}}{9\alpha_{V_{\mathrm{T}}} - 1} \quad \text{and} \quad \mu = 0.5 - \frac{1}{6\alpha_{V_{\mathrm{T}}}}$$

3.2. Devitrification behaviour

A previous work showed that differential thermal analysis (DTA) could be used to determine the dominant crystallization mechanism in glass [12]. In this DTA method, δT_p (the maximum height of the DTA peak at T_p) which is expected to be proportional to the total number of nuclei, is plotted as a function of the glass particle size, the amount of sample and the heating rate remaining constant. For a fixed amount of sample, the ratio of the volume to the total effective surface area of all glass particles increases with increasing particle size. For internal (or surface) dominant crystallization, δT_p should increases (or decreases) with increasing particle size. Likewise, DTA can be considered as a rapid and convenient means of determining nucleation–rate type curves, especially the temperature and time dependence [13]. Hence, for a given particle size, $T_n^{\max}$, the temperature where the nucleation rate is maximum is determined from the plot of the crystallization peak height (δT_p) as a function of the nucleation temperature (T_n), the nucleation time (t_n), the weight sample and the heating rate (Q) being constant for each DTA scan. Furthermore, the changes in δT_p at $T_n^{\max}$ with nucleation time are expected to indicate when the glass is saturated with nuclei.

Considering the kinetic parameters of devitrification, the Avrami's law applies well to isothermal studies [14]. This law may be written as:

$$x = 1 - \exp[-(kt)^n] \tag{1}$$

where x is the volume fraction crystallised after time t, n is the Avrami exponent and k is defined as the apparent reaction rate, which is usually assigned an Arrhenian temperature dependence:

$$k = k_0 \exp(-E/RT) \tag{2}$$

where E is the activation energy describing the overall crystallisation process. After rearrangement of Equation 1, one obtains:

$$\ln[-\ln(1 - x)] = n \ln k + n \ln t \tag{3}$$

Relation (3) gives directly the values of n by plotting $\ln[-\ln(1-x)]$ versus $\ln t$. It should be noted that Equation 1 strictly applies to isothermal studies. However, it is commonly used to describe nonisothermal crystallization for which experimental studies are easier to conduct. Several different treatments have been summarized by Yinnon and Uhlmann [15]. All these methods are based on Equations 1 and 2 and assume a constant heating rate Q in all DTA experiments. On this basis, plotting $\ln[-\ln(1-x)]$ versus $\ln Q$ at a fixed temperature, yields to the n value, the relation being written as:

$$\frac{d[\ln[-\ln(1 - x)]]}{d[\ln\ Q]} = n \tag{4}$$

For the determination of the apparent activation energy for crystallization E, the variety of analytical treatments shows the complexity of the physical problem. In analyzing our crystallization data, we have used the common methods, which relate the dependence between T_p, Q, T_0, and $1/T_p$ where T_0 is the temperature at the beginning of the DTA experiment.

The plots of the following relations give straight lines and the slopes allow the determination of the activation energy:

$$\frac{d\left[\ln\left(T_p^2/Q\right)\right]}{d[1/T_p]} = \frac{E}{R} \tag{5}$$

$$\frac{d\,[\ln Q]}{d\left[1/T_p\right]} = \frac{E}{R} \tag{6}$$

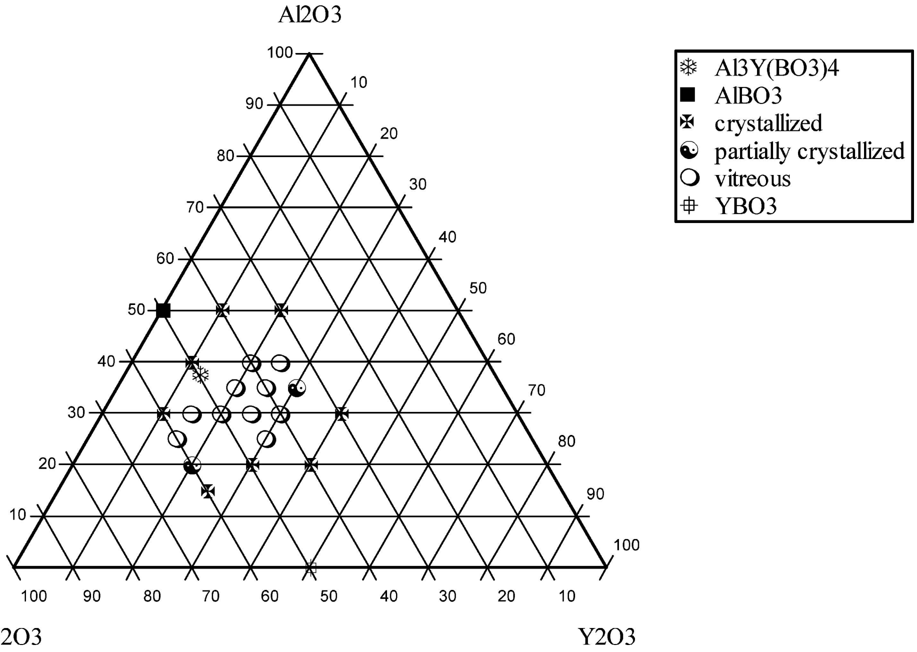

Figure 1 Glass forming region at 1800°C in the ternary composition diagram.

$$\frac{d[\ln(T_p - T_0/Q)]}{d[1/T_p]} = \frac{E}{R} \quad (7)$$

As mentioned above, E is the activation energy describing the overall crystallisation process including nucleation and growth phenomena. Furthermore, Matusita [16] has described a modified Kissinger method to determine E_g the activation energy for crystal growth. The crystallization peak temperature is also monitored as a function of the heating rate, the following relationship is then applied:

$$\ln\left(Q^n/T_p^2\right) = -mE_g/RT_p + \text{constant} \quad (8)$$

where n is the Avrami exponent, and m the dimensionality of the growth. The activation energy for growth is found from the slope ($-mE_g/R$) of the plot corresponding to rel. (8) as a function of ($1/T_p$) with the appropriate values of n and m.

4. Results and discussion

4.1. Physical characteristics

Fig. 1 shows the glass forming region at 1800°C in the ternary composition diagram. Glasses were not chemically analyzed but their composition is expected to be close to the batch composition since the melt do not emitted any visible fumes or vapors during the melting and fining time. The two liquid region has been described for B_2O_3 content greater than 65 mol.% [5] and we have not detected any visual evidence of any phase separation for compositions at the boundary of the immiscibility region. Finally, clear and homogeneous glasses can be obtained for a B_2O_3 content in the range from 35 to 65 mol.%. The $35B_2O_3$-$40Al_2O_3$-$25Y_2O_3$ glass composition (in mol.%) has been selected for our further studies. A DTA plot for this glass, recorded at 10°C/min, is given in Fig. 2.

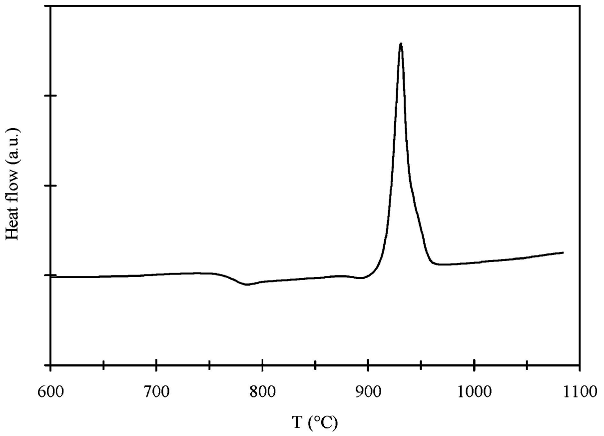

Figure 2 DTA scan recorded at 10°C/min for the $35B_2O_3$-$40Al_2O_3$-$25Y_2O_3$ molar composition.

Some physical characteristics of the as-quenched glass are summarized in Table I and compared with those one obtained for a glass composition in the same ternary

TABLE I Glass transition temperature—Crystallization peak temperature—Density—Thermal expansion coefficient—Vickers microhardness

Glass composition	T_g (°C) ± 1°C	T_p (°C) ± 1°C	d(g.cm^{-3}) ± 0.02	α(10^{-7}.°C^{-1}) ± 1	Hv (Gpa) ± 0.5
This work	774	931	3.40	60	7.2
from [5]	707	–	3.55	75	7.6

TABLE II Dissociation energy per unit volume—Compacity factor—Calculated values for the Young's modulus (E), bulk modulus (K), shear modulus (S) and Poisson's ratio

Compound	G_i (kJ·m^{-3}·10^{-6})	C_i	Elastic moduli
Al_2O_3	120	0.8333	$E = 111$ GPa
Y_2O_3	77.5	0.5403	$K = 85$ GPa
BO_3	3	0.6878	$S = 43$ GPa
BO_4	112.3	0.6878	$\mu = 0.283$

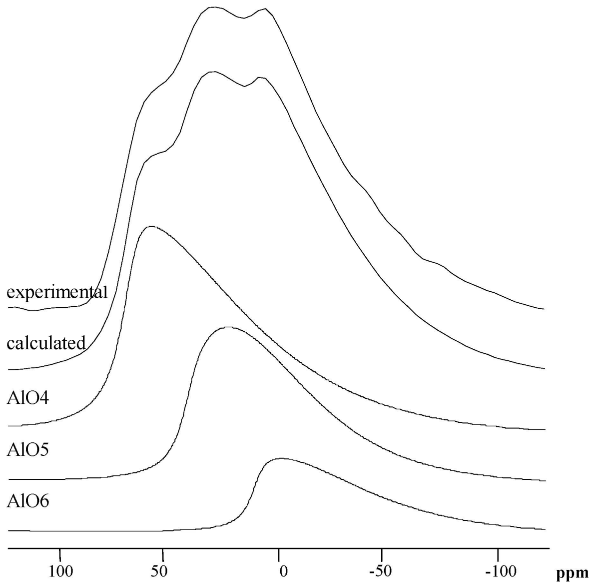

Figure 3 ^{27}Al MAS NMR spectrum.

diagram but with a lower alumina content ($50B_2O_3$-25Al_2O_3-25Y_2O_3) [5]. The glass transition temperature is logically higher but the density and the thermal expansion coefficient (between 20 and 400°C) are lower and the Vickers microhardness is of the same order of magnitude.

The ab-initio determination of the different elastic moduli and of the Poisson's ratio has been performed using the method described previously. The different parameters are given in Table II.

The estimated values of the Young's modulus (E) can be compared with those obtained for calcium and strontium aluminoborate, 100 and 92 GPa respectively [3]. Considering the uncertainty of experimental data and the approximations assumed in the theoretical calculation of the elastic moduli, the general agreement between measured and calculated values has been established as very satisfactory [10]. Consequently we assume that yttrium containing aluminoborate glasses have elastic moduli among the highest obtainable for aluminoborate glasses.

4.2. NMR structural data

The central transition of the ^{27}Al 15 kHz MAS spectrum in the glass studied is presented in Fig. 3. The ^{27}Al spectra validate the presence of three types of neighborhood for Al: four-, five- and six-fold coordination to oxygen [6, 17, 18]. Note that the second order quadrupolar interaction lines are located at the right side of the isotropic chemical shift on a high spinning speed spectrum. The particular asymmetric line shape (trailing high field edge) of each contribution is attributed to the quadrupolar parameter distribution. The relative intensities of the three resolved sites were then evaluated from computer simulation of the experimental spectra [19]. The calculation model assumes a gaussian distribution of the quadrupolar constants ν_Q. In any case η_Q (asymmetric parameter) was fixed at 0.5 since this value does not play any role in the line shapes. The chemical shifts were also fixed for each line because they mainly depend on the number of O around each Al. The fit parameters are gathered in Table III.

TABLE III Parameters of the ^{27}Al and ^{11}B central lines reconstruction where σ values are the broadness of the parameter distributions centered in the ν_Q.values

	Chemical shifts (ppm)	ν_Q.(kHz)	σ (kHz)	Relative intensities (±5%)
Al VI	-17 ± 2	800 ± 20	300 ± 20	20
Al V	13 ± 2	800 ± 20	300 ± 20	30
Al IV	43 ± 2	800 ± 20	300 ± 20	50
BO_3	-17 ± 1	1340 ± 10	60 ± 5	80
BO_4	0 ± 0.2	–	–	20

The central line of the ^{11}B spectrum is depicted in Fig. 4. Two lines are clearly identified with very different quadrupolar lineshapes. In view of their respective chemical shift, these lines are attributed to BO_3 pyramids and BO_4 tetrahedra [8]. The deconvolution was carried out by means of the previously mentioned software [19] and data are gathered in Table III. It appears that, despite the vitreous state of the material, BO_3 type ^{11}B keep an axial asymmetry just slightly smoothed by the structural disorder. This result is in agreement with the oxygen pyramidal symmetry surrounding the ^{11}B probe. On the other

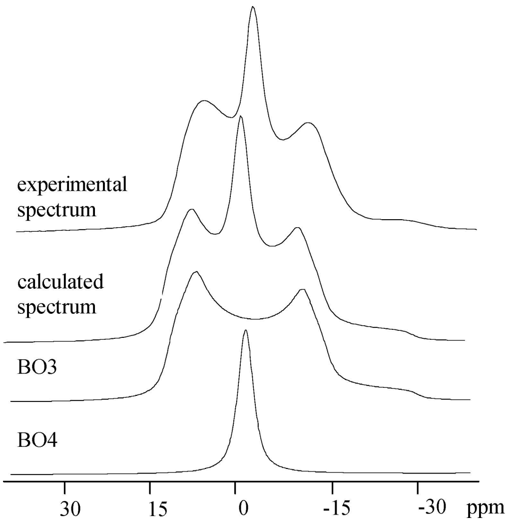

Figure 4 ^{11}B MAS NMR spectrum.

TABLE IV X-ray powder pattern of the new ternary phase (Y,Al)BO_3

2θ (°)	d_{obs} (Å)	$h\,k\,l$	I/I_o
21.397	4.15	0 0 2	55
25.519	3.49	1 0 0	88
27.719	3.22	1 0 1	17
33.554	2.67	1 0 2	100
44.993	2.015	1 1 0	39
50.362	1.811	1 1 2	45
51.260	1.782	1 0 4	41
52.460	1.744	2 0 0	13
57.290	1.608	2 0 2	17
64.489	1.4449	1 1 4	9

hand, the tetrahedral BO_4 type ^{11}B sites possess a higher symmetry and the corresponding line exhibits a simple gaussian shape. Note that BO_3 entities are four times as numerous than BO_4.

4.3. Devitrification behaviour

4.3.1. Phase characterization

The sample has been previously heated to 1020°C at 10°C/min and quenched to room temperature in the DTA apparatus. X-ray powder diffraction data for the crystalline phase occurring during the crystallization thermal event were collected at 25°C. The pattern was scanned over the angular range 10–70°(2θ) with a step length of 0.02°(2θ) and a fixed counting time 2 sec.step^{-1} (see Fig. 5). First, the interrogation of the ICDD-PDF database (2003) reveals apparent isostructural chemically related binary compounds. For pattern indexing, the angular positions from the Bragg reflections were extracted by the pattern decomposition technique using the fitting program FIT available in the software package WINPLOTR [20]. A pseudo-Voigt function was selected to describe individual line profiles. Pattern indexing was carried out by means of the program DICVOL91 [21] based on the dichotomy method [22]. The ten lines observed in the angular range 10–70°(2θ) were indexed with an absolute error of 0.03°(2θ) on the peak positions. The dichotomy method led to a unique hexagonal solution together with correct De Wolff [23] and Smith-Snyder [24] figures of merit, $M_{10} = 134$ and $F_{10} = 47$ (0.0106, 20), respectively. The low ratio $N_{obs}/N_{calc} = 1/2$ is partly due to the low quality of data in terms of diffraction lines broadening and high background noise owing to the additional presence of glass. After a least-squares refinement from the complete set of resolved diffraction lines available, the unit cell dimensions were $a = 4.0289(6)$ Å and $c = 8.295(2)$ Å with $V = 116.61(3)$ Å^3. According to the systematic absent reflections, the most likely space groups were $P6_3/m$ [$M_{10} = 158$ and $F_{10} = 55$ (0.0106, 17)] or $P6_3/mmc$ [$M_{10} = 179$ and $F_{10} = 63$ (0.0106, 15)]. Let us mention that comparison between these results obtained from powder diffraction data for the ternary phase (Y,Al)BO_3 and those given in the literature for the binary rare earth orthoborates $LnBO_3$ provides evidence for strong isostructural relationships based on more 7 than the high-temperature vaterite-type structure [25] that the calcite or aragonite varieties. In the hexagonal form with yttrium, the unit cell parameters given for the revised structure of YBO_3 (PDF file No 88-0356) determined from X-ray single crystal data are $a = 3.776(1)$ Å and $c = 8.806(4)$ Å [$V = 108.74$ Å^3, ρcalc $= 4.512$ g.cm^{-3} and $Z = 2$, S.G. $P6_3/m$]. These recent results have been published long after the study of Newnham *et al.* [26] which had then proposed two other space groups, a disordered $P6_3/mmc$ [PDF file No 74-1929] and an ordered $P6_3/mcm$ hexagonal space groups. The structure consists of a three-dimensional network built up of eightfold coordinated yttrium atoms distributed in the 2 (a) sites symmetry (3) and fourfold coordinated boron forming [BO_4] tetrahedra while in the series of orthoborates, which presents a low-temperature as $LuBO_3$ (PDF file No 72-1053, $V = 233.8$ Å^3, $\rho_{calc} = 6.8$ g.cm^{-3}] [27] or high-pressure as $AlBO_3$ [PDF file No. 75-1108, $V = 237.2$ Å ^{3}, $\rho_{calc} = 3.60$ g.cm^{-3}] [28] calcite-like structure with a rhombohedral symmetry (S.G. $R3\ c$, Z = 6), the oxygen arrangement around the Lu or Al atoms along the triad axis is close to hexagonal-close-packing with triangular-planar BO_3 units. Otherwise, note that no apparent structural properties should be exist with the known ternary rhombohedral orthoborate $YAl_3(BO_3)_4$ (PDF file No. 72-1978, $V = 541.9$ Å^3, $\rho_{calc} = 3.72$ g.cm^{-3}, S.G. R32, $Z = 3$) [29]. No doubt that the detailed chemical composition of the present crystallized variety can not be given because of the low quality diffraction data; nevertheless, by calculating the chemical formula-unit equivalent volume V_{eq} (V_{cell}/Z) for each known varieties used for comparisons, it may be pointed out that the structure of the new compound assuming $Z = 2$ ($V_{eq} = 58.3$ Å^3) appears as less compact than that of $AlBO_3$ [28] which results a value of $V_{eq} = 39.5$ Å^3 ($Z = 6$). The compacity is rather closer than that of the binary phase with yttrium [26] ($V_{eq} = 54.4$ Å^3) which confirms that the new ternary phase (Y,Al)BO_3 would be related to the vaterite-type structure containing aluminum. Nevertheless, it must be kept in mind that the cation Al^{3+} is not known for presenting a flexible coordination polyhedra (from 4 to 6) and consequently for having an eight-fold coordination as Y^{3+} in YBO_3. At the opposite, the yttrium element can easily adopt a six-fold

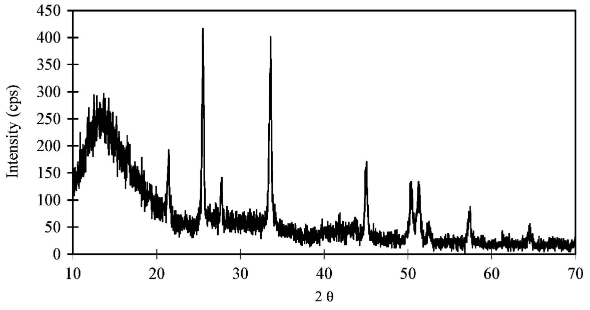

Figure 5 Powder diffraction pattern of the ternary phase (Y,Al)BO_3 obtained at 1020°C according to a heating rate of 10°C.min^{-1} (Note the high diffusion effect due to the presence of a residual glassy phase).

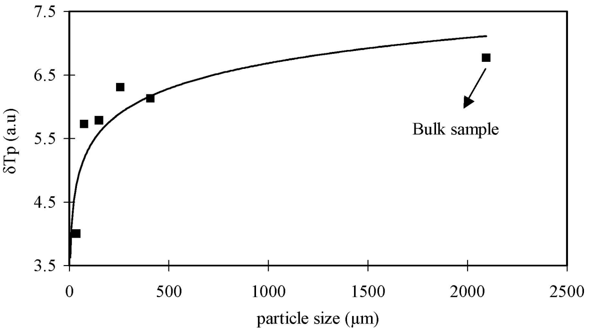

Figure 6 DTA peak height as a function of the particle size of the sample.

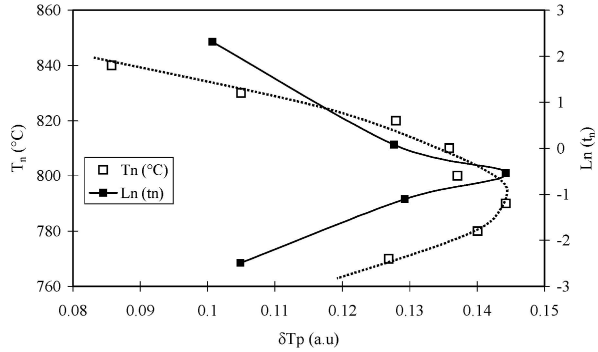

Figure 7 Nucleation temperature and time dependence.

coordination when it is associated with a smaller cation such as Al^{3+}, as for instance in $YAl_3(BO_3)4$ [29]. Moreover, in spite of a significant decrease of the c parameter from YBO_3 to $(Y,Al)BO_3$ ($\Delta c = -0.511$ Å), which can be then explained by the partial substitution from Y^{3+} by Al^{3+} along the c axis, the volume increase occurs due to a change within the (a, b) plane which exhibits a growing surface, i.e. +1.974 $Å_2$. Unfortunately, the quality of the powder data is not good enough to undertake a structure determination.

4.3.2. Determination of the crystallization kinetics

To determine the dominant crystallization mechanism, a single quenched glass was ground and screened to five different particle size ranges in μm, <50, 50–100, 100–200, 200–315, 315–500. These different ranges are designated by the approximate average size in each range (excepted for the first one): 50, 75, 150, 250 and 410 μm. Samples of different particle size, with a constant weight (15 ± 0.1 mg) were heated at 15°C/min from room temperature until crystallization was complete. In addition, a bulk sample for which the diameter of the particle can be estimated from density and weight has been crystallized in the same condition. The estimated experimental error in the measurement of δT_p does not exceed ±2%. The effect of particle size on DSC crystallization peak is shown in Fig. 6.

According to the shape of the curve, the internal crystallisation is the dominant mechanism. Moreover, δT_p can be considered as constant for glass particle size above 100 μm and the dominant crystallization mechanism is the same as for bulk sample. Consequently, in the following sections, only results for samples with a 100–200 μm particle size range will be presented.

Experimental values of the maximum height of the exothermic DTA crystallization peak (δT_p) as a function of nucleation temperature (T_n), are shown in Fig. 7, the nucleation time (t_n) being 30 min. Furthermore, the changes in δT_p at $T_n^{\max}$ with nucleation time are expected to indicate when the glass is saturated with nuclei. In that case, glass particles were nucleated at $T_n^{\max}$ (determined in a first step) for time between 0 and 10 h and then heated at 15°C/min to be sure that crystallization occurs solely from nuclei formed during the isothermal heat treatment. Fig. 7 relates the time dependence of the nucleation rate at $T_n^{\max}$. Then, the most advantageous conditions for nucleation correspond to 790°C and 30 min.

The Avrami exponent of glass samples, for which only non-isothermal nucleation heat treatments were conducted (i.e. the heating times between room temperature and the crystallization peak at various heating rates) has been obtained by plotting ln[−ln(1−x)] versus ln Q (see Fig. 8a) at different temperatures. After a least square treatment, the slopes of the straight lines give the values of n, which are mentioned in Table V.

Concerning the determination of the activation energy value for the overall crystallization phenomenon, we have applied the different analytical methods discussed in Sec-

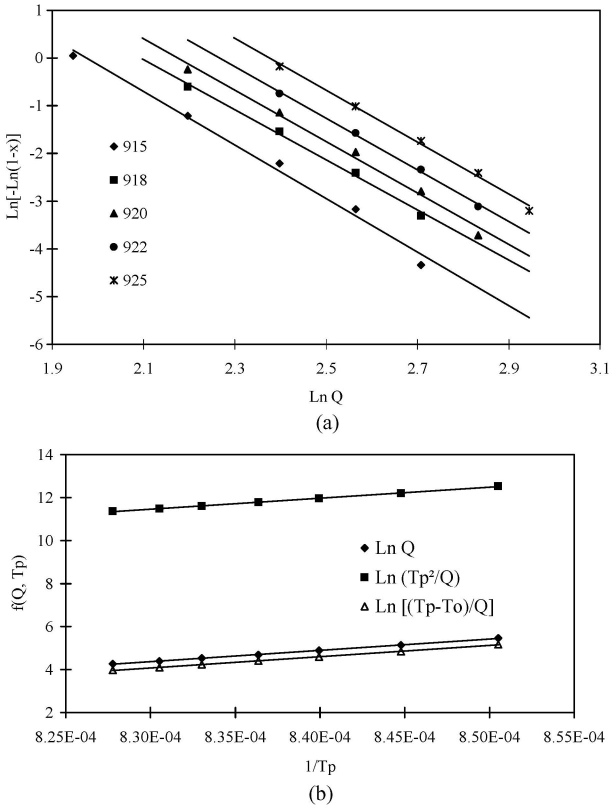

(a)

(b)

Figure 8 (a) Determination of the Avrami exponent (b) Determination of the activation energy for the overall crystallization phenomenon.

TABLE V Values of the Avrami exponent and of the activation energy for the overall crystallization phenomenon

T(°C)	n	R^2	Method	E_a (kJ/mol)	R^2
915	5.61	0.990			
918	5.25	0.996	$\mathrm{Ln}(T_p{}^2/Q)$	428	0.999
920	5.39	0.991	$\mathrm{Ln}[(T_p\text{-}T_0)/Q]$	435	0.999
922	5.41	0.998	Ln Q	438	0.999
925	5.45	0.996			
$<n> = 5.42 \pm 0.10$			$<Ea> = 437 \pm 5$ kJ.mol^{-1}		

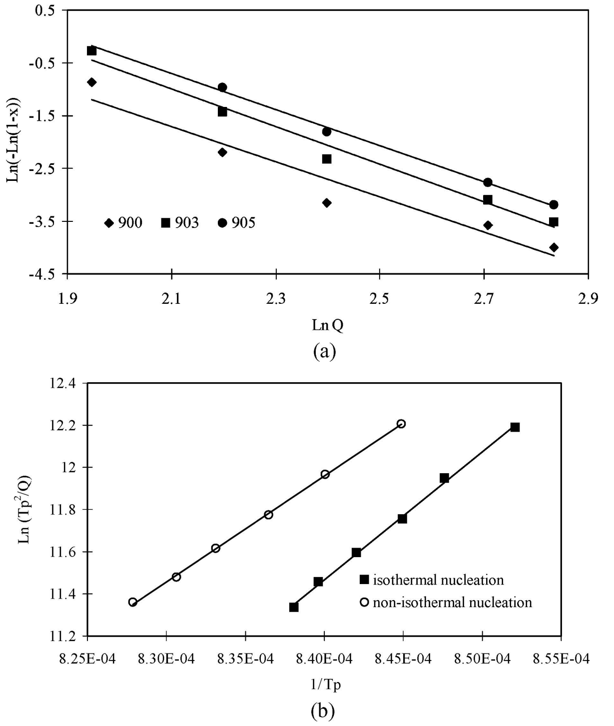

Figure 9 (a) Determination of the Avrami exponent for isothermally nucleated samples (b) Kissinger plots obtained after isothermal nucleation (filled squares) and nonisothermal nucleation (opened circles, data from Fig. 8b).

TABLE VI Values of the Avrami exponent and of the activation energy for cristal growth

T (°C)	n	R^2	$\frac{d\left[\ln\left(T_p^2/Q\right)\right]}{d(1/T_p)}\left(K^{-1}\right)$	60730
900	3.33	0.935	R^2	0.998
903	3.57	0.982	m	3
905	3.43	0.995	$<n>$	3.44
$<n> = 3.44 \pm 0.11$			$E_g = 579 \pm 24$ kJ.mol^{-1}	

tion 3.2 and the results are displayed in Fig. 8b. The plots of $\ln(T_p{}^2/Q)$, ln Q and $\ln[(T_p - T_0)Q]$ versus $1/T_p$ give straight lines and the values for E can be determined from the slopes of the different straight lines after least square treatments. These results are also summarized in Table V.

It is well established that the Avrami exponent may be correlated to the crystallization mechanism. A mean value of 5.42 ± 0.10 indicates that crystallization is three-dimensional and that the nonisothermal saturation of the nucleation sites is not achieved when growth occurs. In the same way, the mean value obtained for E_a (i.e. 437 ± 5 kJ.mol^{-1}) is assumed to be representative of the activation energy of the overall phenomenon including nucleation and growth.

In order to determine the activation energy for crystal growth (E_g), glass samples with a 100–200 μm particle size range, have been nucleated at 790°C during 30 min (i.e. the experimental optimum nucleation conditions). In a first step, we have determined the Avrami exponent (see Fig. 9a) for these nucleated samples, from Equation (4) at different temperatures. These values are summarized in Table VI.

As an evidence, the crystallization of the nucleated glass is three-dimensional and implies, in theory, that $m = n = 3$. The difference between the theoretical and the calculated values of n, may be explained by a slight discrepancy in the experimental data (see the values of the correlation coefficient, R^2, in Table VI) and mainly by the fact that the saturation of the nucleation sites is not entirely accomplished after the heat treatment at 790°C during 30 min. However, the mean value of $3.44(\pm 0.10)$ for the Avrami exponent is largely lower than those one obtained for non-isothermal nucleation of the glass (5.42 ± 0.10), supporting the fact that nucleation and growth do not overlap at any temperature and that the nucleation sites saturation is not obtainable from non-isothermal heat treatment in the case of such an internal crystallization.

According to Equation 8, E_g can be determined from the plot of $\ln(T_p{}^2/Q)$ as a function of the inverse of the crystallization peak temperature. The experimental data are displayed in Fig. 9b with those ones obtained from the non-isothermal nucleation and the calculated value of E_g is given in Table VI. In this study, we have assumed that the crystal growth rate had an Arrhenian temperature dependence. Over the temperature range where the thermo-analytical measurements were carried out, the nucleation was considered as negligible because of the site saturation which has been performed during the isothermal heat treatment. Consequently, a value of 579 ± 24 kJ.mol^{-1} has been obtained for the activation energy for crystal growth, considering a three-dimensional growth ($m = 3$) and a mean value of 3.44 for the Avrami exponent.

5. Conclusion

The glass forming region in the B_2O_3-Al_2O_3-Y_2O_3 composition diagram has been determined at 1800°C. A $35B_2O_3$-$40Al_2O_3$-$25Y_2O_3$ glass composition (in mol.%) has been selected. Different physical characteristics (T_g

$\geq 750°\mathrm{C}$, $E_{\mathrm{cal}} \geq 110$ Gpa, $CTE \leq 60.10^{-7}°\mathrm{C}^{-1}$) confer to this glass matrix a refractory character. This was corroborated by the large proportion of BO_4 and AlO_4 tetrahedral units, 20 and 50% respectively determined from NMR structural data. The devitrification behaviour has also been studied. Diffraction data have shown a new ternary phase (Y,Al)BO_3 related to a vaterite-type structure containing aluminum. Internal crystallization is the dominant mechanism and the most advantageous conditions for nucleation correspond to 790°C and 30 min. Furthermore, a value of $3.44(\pm 0.10)$ for the Avrami exponent obtained in the case of nucleated samples confirms that crystallization is three-dimensional and supports the fact that nucleation and growth do not overlap at any temperature. Moreover, a value of 579 ± 24 kJ.mol^{-1} has been obtained for the activation energy for crystal growth.

References

1. I. N. CHAKRABORTY, J. E. SHELBY and R. A. CONDRATE, *J. Am. Ceram. Soc.* **67**(12) (1984) 782.
2. I. N. CHAKRABORTY, D. E. DAY, J. C. LAPP and J. E. SHELBY, *ibid.* **68**(7) (1985) 368.
3. J. F. MACDOWELL, *ibid.* **73**(8) (1990) 2287.
4. R. K. BROW and D. R. TALLANT, *ibid.* **80**(5) (1997) 1239.
5. H. L. RUTZ, D. E. DAY and C. F. SPENCER, *ibid.* **73**(6) (1990) 1788.
6. D. MASSIOT, B. COTE, F. TAULELLE and J. P. COUTURE, "Application of NMR Spectroscopy to cement Science," edited by Colombet and Grimmer (Gordon and Breach Publishers, 1994) p. 153.
7. C. MAGNENET, D. MASSIOT, I. KLUR and J. P. COUTURE, *J. Mater. Sci.* **35** (2000) 115.
8. K. L. D. MACKENZIE and M. E. SMITH, Multinuclear Solid-state NMR of Inorganic Materials, Pergamon Materials Series (2002) p. 420.
9. A. MAKISHIMA and J. D. MACKENZIE, *J. Non-Cryst. Sol.* **12** (1973) 35.
10. J. ROCHERULLÉ, C. ECOLIVET, M. POULAIN, P. VERDIER and Y. LAURENT, *ibid.* **108** (1989) 187.
11. A. MAKISHIMA and J. D. MACKENZIE, *ibid.* **17** (1975) 147.
12. C. S. RAY and D. E. DAY, *J. Am. Ceram. Soc.* **72** (1990) 439.
13. *Idem., ibid.* **80**(12) (1997) 3100.
14. M. AVRAMI, *J. Chem. Phys.* **8** (1940) 212.
15. H. YINNON and D. R. UHLMANN, *J. Non-Cryst. Sol.* **54** (1983) 253.
16. K. MATUSITA and S. SAKKA, *ibid.* **38** (1980) 741.
17. R. J. KIRKPATRICK and R. K. BROW, *Solid State NMR* **5** (1995) 9.
18. R. K. BROW, *J. Non-Cryst. Sol.* **263/264** (2000) 1.
19. D. MASSIOT, F. FAYON, M. CAPRON, I. KING, S. LE CALVÉ, B. ALONSO, J.-O. DURAND, B. BUJOLI, Z. GAN and G. HOATSON, *Magnetic Resonance in Chemistry* **40** (2002) 70.
20. T. ROISNEL and J. RODRIGUEZ-CARVAJAL, in Proceedings of European Powder Diffraction Conference (EPDIC 7) (2001) vol. 118, p. 378.
21. A. BOULTIF and D. LOUËR, *J. Appl. Crystallogr.* **24** (1991) 987.
22. D. LOUËR and M. LOUËR, *ibid.* **5** (1972) 271.
23. P. M. DE WOLFF, *ibid.* **12** (1968) 60.
24. G. S. SMITH and R. L. SNYDER, *ibid.* **1** (1979) 108.
25. G. CHADEYRON, M. EL-GHOZZI, R. MAHIOU, A. ARBUS and J. C. COUSSEINS, *J. Solid State Chem.* **128** (1997) 261.
26. R. E. NEWNHAM, M. S. REDMAN and R. P. SANTERO, *J. Am. Ceram. Soc.* **46** (1963) 253.
27. S. C. ABRAHAMS, J. L. BERNSTEIN and E. T. KEVE, *J. Appl. Crystallogr.* **4** (1971) 284.
28. A. VEGAS, *Acta Cryst.* **B33** (1977) 3607.
29. E. L. BELOKONEVA et al., *Zh. Strukt. Khim.* **22** (1981) 196.

Received 11 January
and accepted 9 May 2005